bioRxiv preprint doi: https://doi.org/10.1101/2020.08.10.245043; this version posted August 12, 2020. The copyright holder for this preprint (which was not certified by peer review) is the author/funder, who has granted bioRxiv a license to display the preprint in perpetuity. It is made available under aCC-BY-NC 4.0 International license.

Why are rare variants hard to impute? Coalescent models reveal theoretical limits in existing algorithms.

Yichen Si[*] and Sebastian Zöllner[*†,1]

[*]University of Michigan. Department of Biostatistics

[†]University of Michigan. Department of Psychiatry

[1]Corresponding author

bioRxiv preprint doi: https://doi.org/10.1101/2020.08.10.245043; this version posted August 12, 2020. The copyright holder for this preprint (which was not certified by peer review) is the author/funder, who has granted bioRxiv a license to display the preprint in perpetuity. It is made available under aCC-BY-NC 4.0 International license.

Abstract

Genotype imputation is an indispensable step in human genetic studies. Large reference panels with deeply sequenced genomes now allow interrogating variants with minor allele frequency $< 1\%$ without sequencing. While it is critical to consider limits of this approach, imputation methods for rare variants have only done so empirically; the theoretical basis of their imputation accuracy has not been explored. To provide theoretical consideration of imputation accuracy under the current imputation framework, we develop a coalescent model of imputing rare variants, leveraging the joint genealogy of the sample to be imputed and reference individuals. We show that broadly used imputation algorithms includes model miss-specifications about this joint genealogy that limit the ability to correctly impute rare variants. We develop closed-form solutions for the probability distribution of this joint genealogy and quantify the inevitable error rate resulting from the model miss-specification across a range of allele frequencies and reference sample sizes. We show that the probability of a falsely imputed minor allele decreases with reference sample size, but the proportion of falsely imputed minor alleles mostly depends on the allele count in the reference sample. We summarize the impact of this error on genotype imputation on association tests by calculating the r^2 between imputed and true genotype and show that even when modeling other sources of error, the impact of the model miss-specification have a significant impact on the r^2 of rare variants. These results provide a framework for developing new imputation algorithms and for interpreting rare variant association analyses.

bioRxiv preprint doi: https://doi.org/10.1101/2020.08.10.245043; this version posted August 12, 2020. The copyright holder for this preprint (which was not certified by peer review) is the author/funder, who has granted bioRxiv a license to display the preprint in perpetuity. It is made available under aCC-BY-NC 4.0 International license.

1 Introduction

Emerging results from sequencing studies elucidate the impact of rare variants on the etiology of complex diseases [20]. Genome sequencing studies with deep coverage allow directly assessing these variants [10], but such studies are still expensive. As an alternative, array-based technologies can be employed at a substantially lower cost. Commercial genotyping arrays cover a pre-selected set of common variants, and in some cases low frequency variants known to be of interest from previous studies. To recover high resolution genetic information, genotype imputation compares assayed genotypes to a sequenced reference panel, thus leveraging the shared genealogy between genotyped (target) individuals and reference panel to infer unobserved genotypes [16].

Modern imputation methods combined with large reference panels have achieved high accuracy among even low frequency variants. For example, using the TOPMed data as reference, the average imputation quality (r^2) of variants with frequency 0.1% is over 0.90 for both African and European ancestry genomes [23]. Such imputation with high resolution improves the power of genome-wide association studies (GWAS) for low frequency and rare variants, and enables joint analysis across studies with different sets of genotyped variants [4]: Recently, the TOPMed consortium identified a new risk variant for breast cancer by imputing rare variants with minor allele frequency $< 0.5\%$ into the UK Biobank [23]. Such discoveries are enabled by the advent of affordable whole genome sequencing generating large collections of reference haplotypes. To account for the computational challenges resulting from such large reference panels, recent development of imputation algorithms features an efficient pipeline with pre-phasing followed by imputing into haplotypes [4].

Most of these modern imputation methods are based on the Li and Stephens' model [11]. They leverage that haplotypes from unrelated individuals share chromosome segments from a common ancestor. These segments are more similar to each other if their common ancestor is more recent. Among haplotypes in a large reference panel, the haplotype that has the most recent common ancestor with the target haplotype probably also has very similar genotypes as the target. Using a Hidden Markov Model (HMM), the Li and Stephens algorithm models each target haplotype in the study as

bioRxiv preprint doi: https://doi.org/10.1101/2020.08.10.245043; this version posted August 12, 2020. The copyright holder for this preprint (which was not certified by peer review) is the author/funder, who has granted bioRxiv a license to display the preprint in perpetuity. It is made available under aCC-BY-NC 4.0 International license.

an imperfect mosaic of haplotypes from the reference panel. The haplotypes making up this mosaic are inferred to be the most closely related to the target, and thus provide information for unobserved genotype information. The HMM framework is computationally tractable and naturally incorporates recombination and mutation in its transition and emission probabilities.

Simulation studies have shown that imputation quality depends on the imputed variants' allele frequency, genomic context, the size of the reference panel and population demographics [6, 4]. Despite the significant improvements, imputation of rare variants still have high uncertainty. The average squared correlation (r^2) for variants with MAF 0.01% is below 0.5 even with the largest reference from the same continental population [23]. Although simulation studies have the flexibility to mimic a particular imputation setting, they are often hard to generalize and computationally expensive. Alternatively, probabilistic models of the imputation process provide understanding of the basic properties of the imputation process and are therefore easily generalised.

To develop such a probabilistic model for how the the reference provides information about unobserved genotypes in target haplotypes, we need to account for the relatedness between reference and target haplotypes. Kingman's coalescent [9] provides a suitable theoretical framework for modelling the shared genealogy of these haplotypes. The coalescent traces the genealogy back in time, modeling a sequence of events where individuals find their common ancestors (Figure 1). The coalescent time (the time it takes for two or more haplotypes to find their common ancestor) gives a measure of expected genetic dissimilarity, since only mutations occurring more recent than the coalescent time can result in different alleles among those haplotypes.

Some aspects of imputation accuracy have already been explored using coalescent theory. Jewett et al. studied the scenario where the target and reference are sampled from two populations diverged in the past, and derived expected imputation error rate as a function of reference size and divergence time [8]. Huang et al. further included mutation rate and marker density as factors; and analyzed the potential gain in accuracy by choosing the reference panel from a more closely related population[6].

Here we develop a coalescent approach to understand imputation accuracy within population,

bioRxiv preprint doi: https://doi.org/10.1101/2020.08.10.245043; this version posted August 12, 2020. The copyright holder for this preprint (which was not certified by peer review) is the author/funder, who has granted bioRxiv a license to display the preprint in perpetuity. It is made available under aCC-BY-NC 4.0 International license.

focused on rare variants. It is useful to recognize that imputation error has two types of sources: (1) failure to identify haplotypes most closely related to the target as the template and (2) true differences between the template and the target haplotype due to recent mutation events. While improving imputation algorithms may reduce error of the first type, error of the second type is a result of the underlying genealogical relation between the target and the reference sample and how this relationship is modelled by Li and Stephens. Here we focus on modelling the second type of error. Thus we determine the error that is immanent to the Li and Stephens model.

For this purpose, we consider one target haplotype with missing genotype and n fully sequenced haplotypes as references. These $n+1$ observed lineages form the leaves of a binary tree with their (unobserved) ancestors as internal nodes. Intuitively, if the target first finds the most recent common ancestor (MRCA) with a set of reference haplotypes, their genotypes are the most similar to the target thus most informative for imputation. The Li and Stephens algorithm assumes that there is exactly one such most closely related reference haplotype, but we show that this assumption is wrong with probability 1/3.

We compute how often this misspecification leads to an ambiguous or wrongly imputed genotype, assuming the imputation algorithm correctly identifies exactly those haplotypes that are most closely related to the target sample in the reference. We provide the probability of generating a particular imputed dosage conditional on allele frequency of the variant and the size of reference panel. We also quantify the imputation accuracy in terms of the r^2 between the imputed dosage and the true genotype, and show that, as a result of this misspecification, the r^2 largely depends on the allele count in the reference panel, improving only marginally with increased reference size. We assess the impact of population history on these results and use coalescent simulation to confirm our analytic results. Our results provide the minimal size of the reference panel necessary to achieve the desired imputation accuracy for a given allele frequency.

The model we develop here can also be leveraged to improve current imputation algorithms. For example, most imputation algorithms assume that the distance between switching template

bioRxiv preprint doi: https://doi.org/10.1101/2020.08.10.245043; this version posted August 12, 2020. The copyright holder for this preprint (which was not certified by peer review) is the author/funder, who has granted bioRxiv a license to display the preprint in perpetuity. It is made available under aCC-BY-NC 4.0 International license.

haplotypes reflects recombination events and is exponentially distributed [13]. We derive the length distribution of contiguous segments without observable recombination breakpoints, and show that it differs substantially from the exponential assumption by having thicker tails for both very short and long segments.

bioRxiv preprint doi: https://doi.org/10.1101/2020.08.10.245043; this version posted August 12, 2020. The copyright holder for this preprint (which was not certified by peer review) is the author/funder, who has granted bioRxiv a license to display the preprint in perpetuity. It is made available under aCC-BY-NC 4.0 International license.

2 Method

We consider imputing a single target variant for one target haplotype with a reference panel consisting of n reference haplotypes. At each SNP site, all reference haplotypes and the target form a coalescent tree with $n+1$ leaves. This tree is unknown but represents the complete information that imputation can possibly use (Figure 1). For simplicity, we only discuss biallelic sites denoting the ancestral allele as 0 and derived allele as 1. If the target's most recent common ancestor with the reference sample occurs on a branch that is ancestral to $u \geq 1$ reference haplotypes, all u present day descendants of that branch are the most closely related reference haplotypes. We assume that the imputation algorithm identifies these most closely related reference haplotypes, then assigns the mean genotype of them to the target haplotype as the imputation dosage.

Under this assumption, we consider three scenarios: (1) The mutation generating the target variant is ancestral to the time to the most recent common ancestor (TMRCA) of the target haplotype and all its most closely related reference haplotypes. In this case, it will be imputed correctly with dosage 1. (2) The mutation occurred more recently than the TMRCA and the mutation occurred on the branch to the target haplotype. Then the target variant is not polymorphic in the reference sample and will always be falsely imputed to be the ancestral allele. (3) The mutation occurred more recently than the TMRCA and the mutation occurred on the branches to the reference haplotype. Then some or all of the most closely related reference haplotypes carry the derived allele while the template haplotype carries the ancestral allele.

We focus on the third scenario where j of the u most closely related templates carry the derived allele while the target does not. The Li and Stephens model assumes a single closest haplotype, and in the HMM implementation the imputed fractional genotype (dosage) is a weighted average of multiple reference haplotypes based on their posterior probabilities of being that right template. When the u are equivalently close to the target, they are expected to have equal posterior probabilities. Thus the imputed dosage $\hat{g}$ is $\hat{g} = j/u \in (0, 1]$ while the true genotype g is $g = 0$ ("false positive"), resulting in loss of information in downstream analysis.

bioRxiv preprint doi: https://doi.org/10.1101/2020.08.10.245043; this version posted August 12, 2020. The copyright holder for this preprint (which was not certified by peer review) is the author/funder, who has granted bioRxiv a license to display the preprint in perpetuity. It is made available under aCC-BY-NC 4.0 International license.

In the following sections, we derive the probability for all possible (j, u) configuration, conditional on observing the derived allele count j in the whole reference. For simplicity, we distinguish the one target haplotype from the rest n reference ones, making the whole tree size $n+1$, although they are exchangeable under the assumption of homogeneity and random mating. We will always consider time backward with $t = 0$ being the current generation.

2.1 Number of most closely related templates

We first give the probability of having u equally good templates: $P(u; n)$.

We leverage that the probability that a set of k lines coalesce before they coalesce with any line among the rest $n-k$ [21] is

$$q_{k,n-k} = \frac{2(k-1)!(n-k)!}{(k+1)(n-1)!}. \tag{1}$$

The generative process can then be imagined as three steps: u templates coalesce first before their MRCA meets the target; then the resulting branch of size $u+1$ meets the rest of the tree. Finally we sum over all possible sets of u templates.

$$\begin{aligned} P(u; n) &= q_{u+1,n-u} \cdot q_{u,1} \cdot \binom{n}{u} \quad (u < n) \\ &= \frac{2u!(n-u)!}{(u+2)n!} \frac{2(u-1)!}{(u+1)u!} \frac{n!}{(n-u)!u!} \\ &= \frac{4}{u(u+1)(u+2)} \qquad (1 \leq u \leq n-1) \\ P(u = n; n) &= q_{n,1} = \frac{2}{n(n+1)} \end{aligned} \tag{2}$$

The expected number of best templates is close to 2 when the reference is large:

bioRxiv preprint doi: https://doi.org/10.1101/2020.08.10.245043; this version posted August 12, 2020. The copyright holder for this preprint (which was not certified by peer review) is the author/funder, who has granted bioRxiv a license to display the preprint in perpetuity. It is made available under aCC-BY-NC 4.0 International license.

$$
\begin{aligned}
E[u;n] &= \sum_{u=1}^{n} uP(u;n) \\
&= \sum_{u=1}^{n-1} u\frac{4}{u(u+1)(u+2)} + n \cdot q_{n,1} \\
&= \frac{2n}{n+1} \approx 2
\end{aligned}
\tag{3}
$$

Symbol	Meaning
g	True genotype at the imputed locus.
$\hat{g}$	Estimated genotype at the imputed locus.
n	Number of haplotypes in the reference panel.
u	Number of most closely related haplotypes (MCRH) in the reference panel.
j	Number of the rare allele in the reference panel.
k	Number of lines remaining on the tree just after all MCRH have reached their MRCA.
d	Number of lines remaining on the tree when the target haplotype coalesces with one ancestor of the reference haplotypes.
l	Length of an internal branch.
m	Number of mutation events on a particular branch.

Table 1: Notation for key quantities

2.2 High certainty error

We now derive the probability of imputing the target to carry the mutation with dosage $\hat{g} = 1$ while the truth is $g = 0$, conditional on the observed derived allele count in the reference panel: $P(\hat{g} = 1, g = 0|j;n)$. This happens when the target haplotype first coalesces with a branch (l) of size j carrying a mutation (Figure 1a).

bioRxiv preprint doi: https://doi.org/10.1101/2020.08.10.245043; this version posted August 12, 2020. The copyright holder for this preprint (which was not certified by peer review) is the author/funder, who has granted bioRxiv a license to display the preprint in perpetuity. It is made available under aCC-BY-NC 4.0 International license.

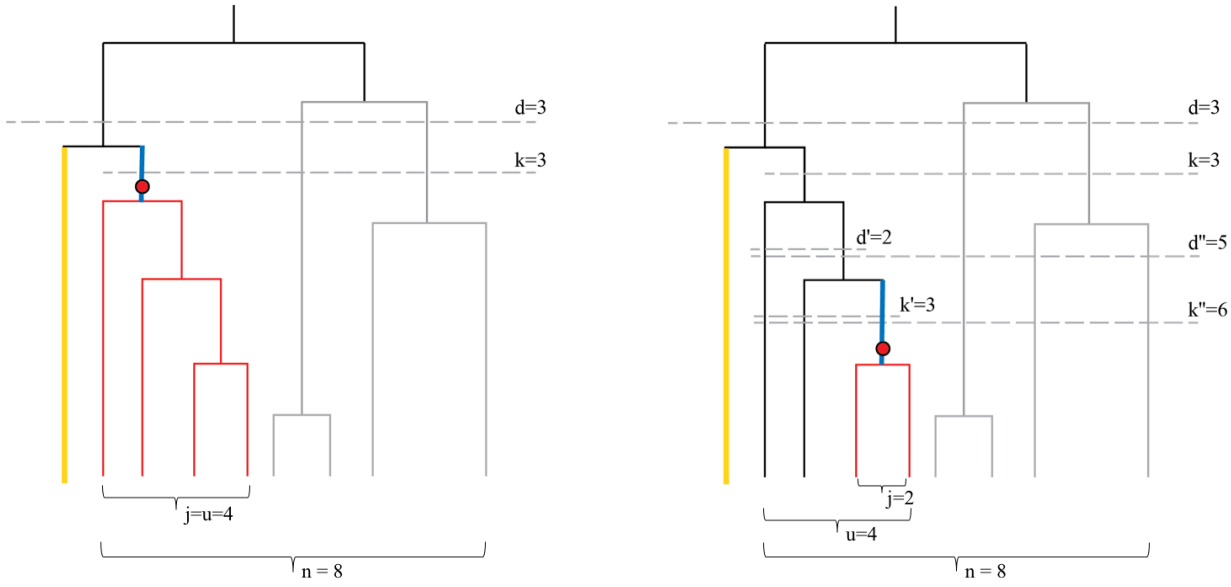

(a) $\hat{g} = 1, g = 0$ **(b)** $\hat{g} = 0.5, g = 0$

Figure 1: Coalescent tree with one target haplotype (yellow line) and a reference panel with n haplotypes. Red lines are haplotypes carrying a mutation that occurs on the blue branch, represented by the red dot. Gray horizontal dashed line indicates the time interval where an event of interest occurs. a) The special case where the target is imputed to have the derived allele, $\hat{g} = 1$ but $g = 0$, even in the best possible imputation scenario. b) An example of the general situation: $u = 4$ reference haplotypes are equally close to the target, $j = 2$ of which carry the mutation, resulting in $\hat{g} = 0.5$ but $g = 0$.

Throughout the following derivation, we use the number of ancestral lines for the current day sample to keep track of coalescent time and to connect topology and branch lengths. We first introduce some quantities useful for our derivation:

Let $P(j, k; n)$ be the probability for j lines to reach their MRCA at the coalescent event that reduces the overall number of ancestral lines from $k + 1$ to k, without any of the j lines coalescing with any of the $n - j$ other lines first. Let $P_0(n, d)$ be the probability for one line to encounter no coalescent event for (at least) the first $n - d$ events. Let $P(m \geq 1|l)$ be the probability of having at least one mutation event on a branch with length l, and let $P(L = l|k, d; n)$ be the probability density function for the length of one internal branch starting when there are k lines left and ending when there are d lines left, in a tree of size n. Using these terms, we can now calculate

$$P(\hat{g} = 1, g = 0|j; n) = \frac{P(\hat{g} = 1, g = 0, j; n)}{P(j; n)}$$

bioRxiv preprint doi: https://doi.org/10.1101/2020.08.10.245043; this version posted August 12, 2020. The copyright holder for this preprint (which was not certified by peer review) is the author/funder, who has granted bioRxiv a license to display the preprint in perpetuity. It is made available under aCC-BY-NC 4.0 International license.

We calculate the joint probability $P(\hat{g}=1, g=0, j; n)$ in the following three steps by conditioning on d and k (Eq. 4, Figure 1a). We calculate $P(j;n)$ by adapting the second step (Eq. 5).

1) To coalesce in the $(n-d+1)th$ coalescent event, when d lines remain on the tree, the target haplotype cannot coalesce in the first $n-d$ events: $P_0(n+1, d+1)$.

2) A branch of size j ancestral to all most closely related reference haplotypes arises in the reference at the $(n-k)th$ event $(P(j,k;n))$ and encounters a mutation before it coalesces with the target branch in event $n-d+1$ $(g(k,d;n))$. Here the probability for a mutation to occur on that particular branch is computed by integrating over all possible branch length l given k and d:. $g(k,d;n) = \int_{l=0}^{l=\infty} P(m \geq 1|l)P(L=l|k+1,d;n+1)dl$.

3) The size-j branch does not coalesce till the $(n-d)th$ event and then coalesces with the target: $P_0(k,d) \cdot \frac{1}{\binom{d+1}{2}}$.

Multiplying the probabilities of these sequential events and summing over all possible values of d, k give the joint probability:

$$\begin{aligned} &P(\hat{g}=1, g=0, j; n) \\ &= \sum_{k=2}^{n-j+1} \sum_{d=2}^{k} P_0(n+1, d+1) \cdot P(j,k;n) \cdot \int_{l=0}^{l=\infty} P(m \geq 1|l)P(L=l|k+1,d;n+1)dl \ \cdot P_0(k,d)\frac{1}{\binom{d+1}{2}} \end{aligned} \tag{4}$$

$$\begin{aligned} &P(j;n) \\ &= \sum_{k=2}^{n-j+1} \sum_{d=1}^{k-1} P(j,k;n) \cdot \int_{l=0}^{l=\infty} P(m \geq 1|l)P(L=l|k,d;n)dl \ \cdot P_0(k,d+1)\frac{d}{\binom{d+1}{2}} \end{aligned} \tag{5}$$

To compute $P(j,k;n)$, define $H(n,k) := \binom{n}{2}\binom{n-1}{2}\cdots\binom{k+1}{2}$, the number of possible configurations of the topological history for n lines to coalesce till there are k ancestral lines left. Then

$$\begin{aligned} P(j,k;n) &= \frac{\binom{n}{j}H(j,1)H(n-j,k-1)\binom{n-k-1}{j-2}}{H(n,k)} \\ &= \frac{\binom{n-k-1}{j-2}}{\binom{n-1}{j}}\frac{(k-1)k}{j}. \end{aligned} \tag{6}$$

Next we consider the integral corresponding to the mutation event $g(k,d;n)$ (Eq. 7). Let $E[T_i;n]$

bioRxiv preprint doi: https://doi.org/10.1101/2020.08.10.245043; this version posted August 12, 2020. The copyright holder for this preprint (which was not certified by peer review) is the author/funder, who has granted bioRxiv a license to display the preprint in perpetuity. It is made available under aCC-BY-NC 4.0 International license.

denote the expected time for the number of ancestral lines to go from i to $i-1$ in the coalescence process for a sample of n current haplotypes , which depends on the population history model. Thus, $g(k,d;n)$ depends on mutation rate μ and expected coalescent time intervals $E[T_k;n]$, which can be numerically computed [14] or approximated by Monte Carlo.

$$\begin{aligned} g(k,d;n) &= \int_{l=0}^{l=\infty} P(m \geq 1|l)P(L=l|k,d;n)dl \\ &= \int_{l} (1-e^{-l\mu})P(L=l|k,d;n)dl \\ &= E[1-e^{-l\mu}|k,d;n] \\ &\approx \mu E[l|k,d;n] \\ &= \mu \sum_{i=d+1}^{i=k} E[T_k;n] \end{aligned} \tag{7}$$

Substituting Eq.6,7 and $P_0(k,d) = \frac{d(d-1)}{k(k-1)}$ into Eq. 4,7, we now have the conditional probability fully defined:

$$\begin{aligned} &P(\hat{g}=1, g=0|j;n) \\ &= \frac{\frac{1}{n(n+1)}\sum_{k=2}^{n-j+1} P(j,k;n)\frac{1}{(k-1)k}\sum_{d=2}^{k} d(d-1)\ g(k+1,d;n+1)}{\sum_{k=2}^{n-j+1} P(j,k;n)\frac{1}{(k-1)k}\sum_{d=1}^{k-1} d\ g(k,d;n)} \end{aligned} \tag{8}$$

Following similar logic as above, we then consider the conditional probability distribution for fractional dosages. We derive $P(\hat{g}=j/u, g=0|j;n)$, the probability of having u equally closely related best templates, j of which carry the mutation, for a target actually carrying the ancestral allele, conditional on observing the derived allele count as j in a reference of size n (figure 1b). Details of derivation are in the Appendix.

2.3 Modelling r^2 as a function of miss-identification proportion

The above derivation fully characterizes the distribution of the imputed dosages assuming we perfectly identify the optimal templates. While it is difficult to model all the possible sources of error in the

bioRxiv preprint doi: https://doi.org/10.1101/2020.08.10.245043; this version posted August 12, 2020. The copyright holder for this preprint (which was not certified by peer review) is the author/funder, who has granted bioRxiv a license to display the preprint in perpetuity. It is made available under aCC-BY-NC 4.0 International license.

real imputation process, we can use the total weight (q) attributed to haplotypes outside the set of most closely related templates to measure the identification error. Here we derive its influence on the square of correlation coefficient (r^2) between the true genotype and imputed dosage.

Let g be the true genotype, 1 for the derived allele and 0 for the ancestral allele; let f be the derived allele frequency, so $E[g] = f$. Let $\tilde{g}$ and $\hat{g}$ be the imputed dosage with and without misidentification respectively.

Let z be the random variable representing the proportion of carriers of the minor allele among the sub-optimal templates contributing to the imputed dosage, so that $\tilde{g}$ can be modeled as a mixture $\tilde{g} = (1-q)\hat{g} + qz$. If we assume that the sub-optimal templates are sampled at random from the population and each of the suboptimal templates is given equal weight, z is the average genotype of m random haplotypes, so $E(z) = f$ and $V(z) = V(g)/m = f(1-f)/m$.

When the optimal templates for a target sample provide the perfect information ($\hat{g} = g$), misidentified templates may be the alternate allele and therefore increase imputation error. However, where the target sample carries the ancestral allele but some of its optimal templates carry the derived allele, sub-optimal templates attenuate the resulting error. Nevertheless, here we show that in expectation imputation error will always reduce the correlation between the true and the imputed genotype. Let's express $r^2_{g,\tilde{g}}$ in terms of quantities regarding the theoretical imputed dosage $\hat{g}$.

$$\begin{aligned} \tilde{g} &= (1-q)\hat{g} + qz \\ \implies \tilde{r}^2_{g,\tilde{g}} &= \frac{Cov(g,\tilde{g})^2}{V(g)V(\tilde{g})} = \frac{((1-q)Cov(g,\hat{g}) + qCov(g,z))^2}{V(g)V((1-q)\hat{g} + qz)} \\ &= \frac{Cov(g,\hat{g})^2 + \frac{2q}{1-q}Cov(g,\hat{g})Cov(g,z) + \frac{q^2}{(1-q)^2}Cov(g,z)^2}{V(g)V(\hat{g}) + \frac{2q}{1-q}V(g)Cov(\hat{g},z) + \frac{q^2}{(1-q)^2}V(g)V(z)} \end{aligned} \tag{9}$$

Comparing to the theoretical $r^2_{g,\hat{g}} = \frac{Cov(g,\hat{g})^2}{V(g)V(\hat{g})}$:

$$\frac{\tilde{r}^2_{g,\tilde{g}}}{r^2_{g,\hat{g}}} = \frac{(1-q)^2 + 2q(1-q)\frac{Cov(g,z)}{Cov(g,\hat{g})} + q^2(\frac{Cov(g,z)}{Cov(g,\hat{g})})^2}{(1-q)^2 + 2q(1-q)\frac{Cov(\hat{g},z)}{V(\hat{g})} + q^2\frac{V(z)}{V(\hat{g})}}. \tag{10}$$

bioRxiv preprint doi: https://doi.org/10.1101/2020.08.10.245043; this version posted August 12, 2020. The copyright holder for this preprint (which was not certified by peer review) is the author/funder, who has granted bioRxiv a license to display the preprint in perpetuity. It is made available under aCC-BY-NC 4.0 International license.

Since $\hat{g}$ is based on a few reference haplotypes and equal to g with large probability, we can reasonably assume $Cov(g, z) \approx Cov(\hat{g}, z)$, $Cov(g, \hat{g}) \approx V(g)$ and $Cov(g, z) < Cov(g, \hat{g})$ (misidentified haplotypes are more distant). Therefore the middle terms in the numerator and denominator of Eq. 10 are approximately equal; the difference between the r^2's is governed by the last terms, which have a ratio strictly smaller than one: $\frac{Cov(g,z)^2}{Cov(g,\hat{g})^2}\frac{V(\hat{g})}{V(z)} = \frac{Cor(g,z)^2}{Cor(g,\hat{g})^2} < 1$.

If misidentified haplotypes are close to random draws from all reference haplotypes ($Cov(g, z) \approx 0$), the ratio simplifies to

$$\frac{\tilde{r}^2_{g,\tilde{g}}}{r^2_{g,\hat{g}}} \approx \frac{(1-q)^2}{(1-q)^2 + q^2\frac{V(z)}{V(\hat{g})}} < 1. \tag{11}$$

In practice, the sub-optimal templates contributing to the imputed dosage are more likely to be from lineages closer to the target, so their effect on imputation accuracy would be smaller than that from the above assumptions.

2.4 Length of haplotype before the next recombination breakpoint

Next we aim to derive the distance between consecutive recombination events on an external branch. For the purpose of modelling imputation, these distances represent the lengths of segments that are copied from the same haplotype. Let X be the genetic distance to the next observed recombination event on the target, and T be the length of its corresponding external branch. We calculate $f_X(x) = \int f_{X|T}(x)f_T(t)dt$ (we will use $f(\cdot)$ for continuous and $P(\cdot)$ for discrete distributions). Similar to above, we compute the probability density function of T by considering it first coalesces at the $(n+1-k)$th event. $T|k$ is the sum of $n+1-k$ coalescent time intervals, thus following a convolution distribution as the sum of $n+1-k$ exponential with different rates. Conditional on T, X follows an exponential distribution with rate $2T$ since a recombination event on either the current template

bioRxiv preprint doi: https://doi.org/10.1101/2020.08.10.245043; this version posted August 12, 2020. The copyright holder for this preprint (which was not certified by peer review) is the author/funder, who has granted bioRxiv a license to display the preprint in perpetuity. It is made available under aCC-BY-NC 4.0 International license.

or the target haplotype results in a switch of template.

$$\begin{aligned} f_{X|T}(x) &= 2Te^{-2Tx} \\ f_{T|k}(t) &= f_{T_{n+1}+\cdots+T_{k+1}}(t) \\ \Rightarrow f_{X|K}(x|k) &= \int_{t=0}^{\infty} f_{T_{n+1}+\cdots+T_{k+1}}(t) f_{X|T}(x|t)dt \\ &= E_{T|k}[2Te^{-2Tx}] \qquad (T|k \sim f_{T_{n+1}+\cdots+T_{k+1}}) \end{aligned} \tag{12}$$

When population size is constant, $E_{T|k}[2Te^{-2Tx}] = \frac{dMGF_T(y)}{dy}|_{y=-2x}$, where MGF_T s the moment generating function of the hypoexponential distribution $T|k$. When population size changes through time so time intervals are correlated, we can approximate the expected value with $2E[T|k]e^{-2E[T|k]x}$ and compute $E[T|k]$ with Monte Carlo.

The probability for a haplotype to first coalesce at the $(n+1-k)$th event is $P_0(n+1,k+1)\frac{k}{\binom{k+1}{2}}$, with $P_0(n+1,k+1)$ being the probability of not coalescing with any lineage in the first $(n-k)$ events (starting from total sample size $n+1$). Therefore we have the distribution of X is

$$f_X(x) = \sum_{k=1}^{n} P_0(n+1,k+1)\frac{k}{\binom{k+1}{2}} f_{X|K}(x|k) \tag{13}$$

$$= \frac{2}{n(n+1)} \sum_{k=1}^{n} k \cdot f_{X|K}(x|k) \tag{14}$$

2.5 Simulation

We performed a standard Kingman coalescent simulation under population history models suggested by recent studies (detailed in the Results). We simulate size-$(n+1)$ trees with n varying from 500 to $50k$. For each generated tree, we keep track for all subtree configurations $(1+u(j))$ (one external branch first coalesces with a branch of size u, which contains a branch of size j) of interests, and record the length of this size j branch. The sum of all such relevant branch lengths in the tree divided by the number of present haplotypes $n+1$ is one realization of the joint probability $P(\hat{g} = j/u,\ g = 0,\ j; n)$, which will then be approximated by averaging such realizations over all

bioRxiv preprint doi: https://doi.org/10.1101/2020.08.10.245043; this version posted August 12, 2020. The copyright holder for this preprint (which was not certified by peer review) is the author/funder, who has granted bioRxiv a license to display the preprint in perpetuity. It is made available under aCC-BY-NC 4.0 International license.

simulated trees. To approximate the probability of observing j derived alleles in the reference panel, we simulated another independent set of trees of size n and summed over the lengths of all size j branches to get sample frequency spectrum. We present results from $50k$ independent simulations under each parameter setting throughout this article.

bioRxiv preprint doi: https://doi.org/10.1101/2020.08.10.245043; this version posted August 12, 2020. The copyright holder for this preprint (which was not certified by peer review) is the author/funder, who has granted bioRxiv a license to display the preprint in perpetuity. It is made available under aCC-BY-NC 4.0 International license.

3 Results

We derived an analytical approach to calculate the impact of model misspecification of the current imputation framework with our coalescent model on rare variants (see the Method). Assuming a Li and Stephens model[11] based imputation algorithm correctly identifies all and only those haplotypes in the reference that are most closely related to the target sample, we calculated the theoretical error rate as a function of reference size n and the derived allele count. Using coalescent simulations, we confirm the analytical results, and incorporate general population models.

3.1 The number of closest template haplotypes

In the coalescence context, identifying a single reference haplotype that is most similar to the target haplotype is equivalent to selecting the reference haplotype that has the most recent common ancestor with the target haplotype or, equivalently, whose lineage is the first to coalesce with the target. However, by the time this lineage coalesces with the target, it may be ancestral to multiple reference haplotypes (Figure 1a). In this case, those reference haplotypes are equally closely related with the target, each of them in expectation providing the same amount of information for imputing the target sample. Thus, the model assuming one single best template is misspecified.

The probability for the target haplotype to first coalesce with a lineage having u reference descendants is

$$P(u) = \frac{4}{u(u+1)(u+2)}, (1 \leq u \leq n-1). \tag{15}$$

This probability only depends on the topology of the coalescent tree, independent of the population history (see the Method). Interestingly, the probability distribution of the number of best matches does not depend on the size of the reference panel (n), except for the extreme case $u = n$, where the entire reference has equal genetic distance to the target. In that case, $P(u = n) = \frac{2}{n(n+1)}$. The expected number of most closely related reference haplotypes $E(u) = 2 - \frac{2}{n+1}$, approaching 2 as the size of the reference panel increases.

bioRxiv preprint doi: https://doi.org/10.1101/2020.08.10.245043; this version posted August 12, 2020. The copyright holder for this preprint (which was not certified by peer review) is the author/funder, who has granted bioRxiv a license to display the preprint in perpetuity. It is made available under aCC-BY-NC 4.0 International license.

From equation (15), we see that with probability $\frac{2}{3}$, the target haplotype first coalesces with an external branch ($u = 1$) and the reference contains exactly one best match. Thus, the Li and Stephens model of exactly one best template is misspecified with probability $\frac{1}{3}$. The probability of u equally good templates drops rapidly with increasing u (Table 2). With probability $\frac{1}{6}$, the target haplotype first coalesces with an internal branch with two descendants in the reference ($u = 2$), while the probability is 0.0108 that the target haplotype first coalesces with an internal branch with more than 10 descendants in the reference ($u > 10$).

No. Templates	1	2	3	4	5	6	7	8	9	10
Prob.	0.6667	0.1667	0.0667	0.0333	0.0190	0.0119	0.0079	0.0056	0.0040	0.0030

Table 2: Probability of having multiple reference haplotypes (No. Templates) most closely related to the target haplotype. In expectation, each of these haplotypes provides the same amount of information for imputation.

3.2 Impact on imputation accuracy

As we have just demonstrated, the model assumption that each target haplotype has a single most closely related template haplotype is a model misspecification for 1/3 of the genome where multiple template haplotypes are most closely related to the target haplotype. This model misspecification contributes to imputation error beyond the typical source of error created by failing to identify the most closely related haplotype. To isolate this additional error, we now evaluate the imputation of a missing genotype assuming that all most-closely related haplotypes are correctly identified but analyzed under a model that assumes a single best haplotype. In this scenario, imputation algorithms will correctly impute all non-singleton variants if the target haplotype has a single most closely related template haplotype. Imputation errors can only occur if the target haplotype has more than one most closely related template haplotype; i.e. a model misspecification. In this case, imputation algorithms consider all these template haplotypes to be equally likely to be the "best" template. Accordingly, it will interpret identifying multiple equally close templates as uncertainty in identifying the best template. For variants that differ between these template haplotypes, the imputed genotype is then usually the average of the derived allele counts (DAC) of those templates, a fractional genotype

bioRxiv preprint doi: https://doi.org/10.1101/2020.08.10.245043; this version posted August 12, 2020. The copyright holder for this preprint (which was not certified by peer review) is the author/funder, who has granted bioRxiv a license to display the preprint in perpetuity. It is made available under aCC-BY-NC 4.0 International license.

(dosage). Thus, for one given target haplotype carrying the ancestral allele to be imputed with a non-zero DAC dosage (false positive), some of its templates have to carry the derived allele.

While the probability of this misspecification is independent of population history, the probability of a mutation event causing an imputation error depends on the history of the population template and target haplotypes are sampled from. In our primary analysis we consider a population history model approximating European population history [19][18]. Starting from an ancestral population with effective population size 10^4, it undergoes a bottleneck with $N_e = 2 \cdot 10^3$ for 100k years (approximately 3450 generations), then grows with an accelerated rate (faster than exponential growth [15]) to $N_e = 10^7$ during the most recent 10k years. The effect of the model parameters on the following results is marginal within a model space reasonable for human population (Appendix B).

We first consider the special case where all template haplotypes that are most closely related to target carry the derived allele, while the target haplotype carries the ancestral allele. In this case, the imputed dosage of the derived allele is 1 when the truth is 0 (Figure 1A). By integrating over all possible tree shapes and branching times (see the Method), we calculated the probability for this configuration for reference sample sizes of 500, 5000, 20,000 and 50,000 individuals. We verified all results using computer simulations. Across all considered reference sizes, the probability of this completely wrong imputation for one imputed haplotype is small ranging from 10^{-3} to $< 10^{-6}$ (Figure 2A, Table 3). Holding reference size constant, this probability decreases with rising DAC. Similarly, holding DAC constant, this probability of imputation error decreases with increasing number of templates.

To put these error rates in relationship with the number of true carriers of the derived allele, we assume that the derived allele frequency in the target population is the same as the derived allele frequency in the reference population. For instance, consider a site with two copies of the derived allele in a reference of 500 individuals (MAF 0.002). For this site, we expect to impute one individual as false carrier for every 1210 individuals (Figure 2). Among these 1210 individuals, we also expect 4.84 true carriers of this variant assuming the same MAF in the target population. Thus, for variants

bioRxiv preprint doi: https://doi.org/10.1101/2020.08.10.245043; this version posted August 12, 2020. The copyright holder for this preprint (which was not certified by peer review) is the author/funder, who has granted bioRxiv a license to display the preprint in perpetuity. It is made available under aCC-BY-NC 4.0 International license.

that are doubletons in a reference sample of 500 individuals, about one in six imputed rare alleles will be a false positive (Table 3). More generally, for a fixed derived allele count in the reference, the probability of falsely imputing the derived allele decreases with increasing reference size while the number of true carriers of the derived allele also decreases. As a result, the proportion of falsely imputed derived alleles decreases only moderately with increasing reference size. For example, for variants that are doubletons in the reference, the proportion of false positive derived alleles decreases only from 17.5% for a reference size of 500 to 14.7% for a reference size of 50,000.

If we now consider the more general case where at least one of template among the haplotypes most closely related to the target carry the derived allele while the target carries the ancestral allele (dosage 0). In this case the imputed dosage $\hat{g} > 0$ (Figure 2). Across reference sizes of 500, 5000, 20,000 and 50,000 individuals, we calculated the probability of $\hat{g} > 0$ for each imputed haplotype. This probability is notably larger than the probability of falsely imputing dosage 1, ranging from $\sim 10^{-3}$ to $\sim 10^{-5}$ for doubletons (with DAC 2, Figure 2b). This probability decreases with rising derived allele count and increasing reference size.

From these probabilities, we calculate the expected number of haplotypes carrying the ancestral allele ($g = 0$) that are falsely imputed to have either a non-zero derived allele dosage ($\hat{g} > 0$) or a dosage $\hat{g} > 0.5$ or a dosage of 1 for every million target individuals (Table 3). Haplotypes with $\hat{g} > 0.5$ represent cases where a "best-guess" imputation algorithm would infer the alternate allele. Beyond the previously described impact of derived allele count and reference size, these results show that for DAC < 5, about half of all falsely imputed derived alleles have a dosage > 0.5. This observation can be explained by the fact that for a given DAC, observing a dosage < 0.5 requires a larger number of equally good templates than observing a larger dosage. As large numbers of equally good templates are rare (Table 2), the proportion of higher dosage among all falsely imputed non-zero dosages increases with the DAC.

bioRxiv preprint doi: https://doi.org/10.1101/2020.08.10.245043; this version posted August 12, 2020. The copyright holder for this preprint (which was not certified by peer review) is the author/funder, who has granted bioRxiv a license to display the preprint in perpetuity. It is made available under aCC-BY-NC 4.0 International license.

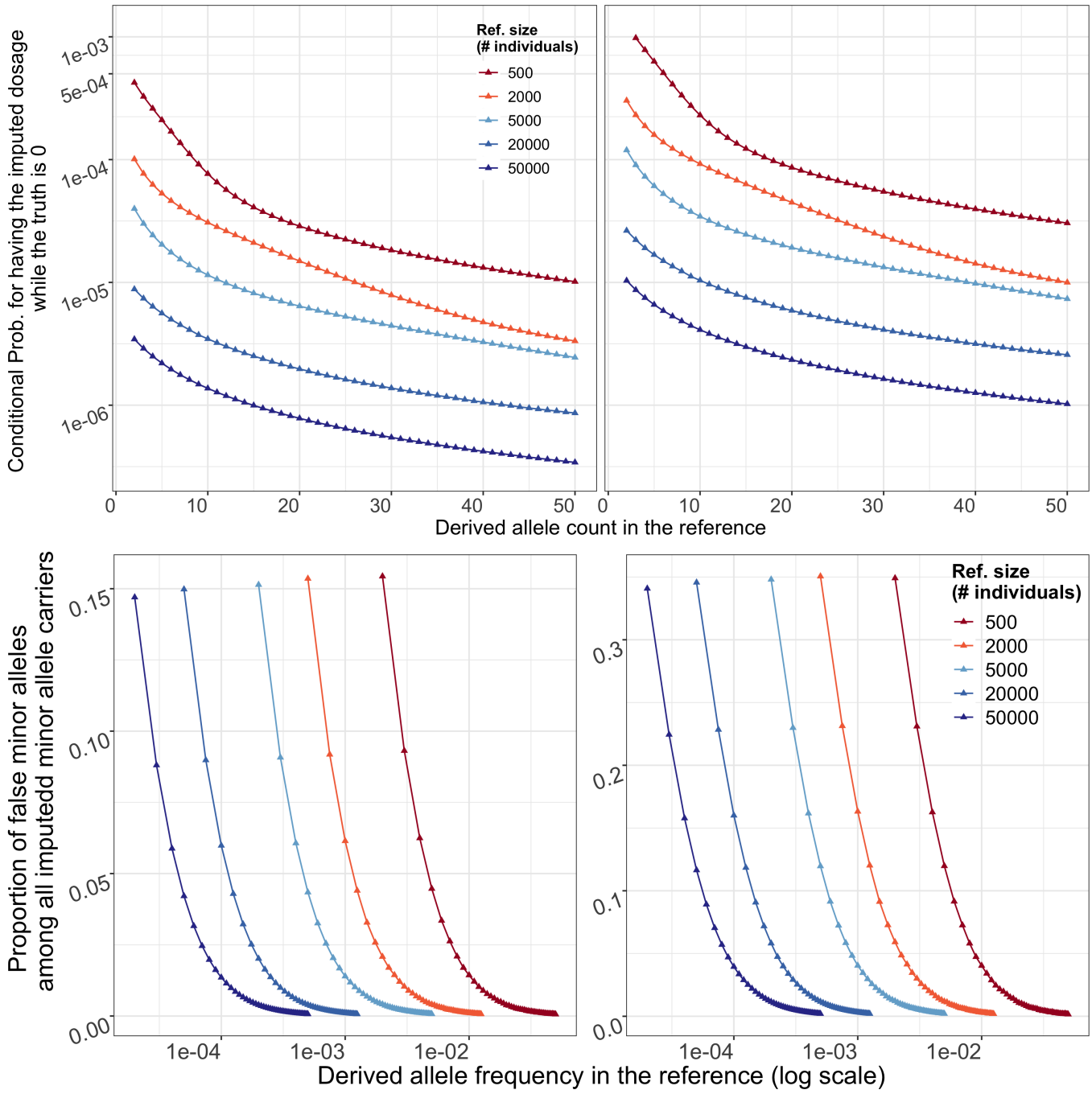

Figure 2: Upper panel: False discovery rate among non-carriers. Given a target haplotype carrying the ancestral allele, the probability (y-axis, in log scale) of having a) all the most closely related reference haplotype in the reference panel carrying the derived allele thus an estimated dosage 1; or b) having non-zero estimated dosage for the derived allele. Lower panel: false positive among all imputed carriers. For a target sample, the proportion (y-axis) of c) non-carrier haplotypes having estimated dosage or d) haplotypes with non-zero dosage among all haplotypes with imputed dosage falling in the corresponding category. Both results are conditional on the derived allele frequency in the reference (x-axis); color indicates the size of reference panel, in the number of individuals. Results for reference size below 20,000 are from analytical calculation while those for 20,000 and 50,000 are from coalescence simulations.

bioRxiv preprint doi: https://doi.org/10.1101/2020.08.10.245043; this version posted August 12, 2020. The copyright holder for this preprint (which was not certified by peer review) is the author/funder, who has granted bioRxiv a license to display the preprint in perpetuity. It is made available under aCC-BY-NC 4.0 International license.

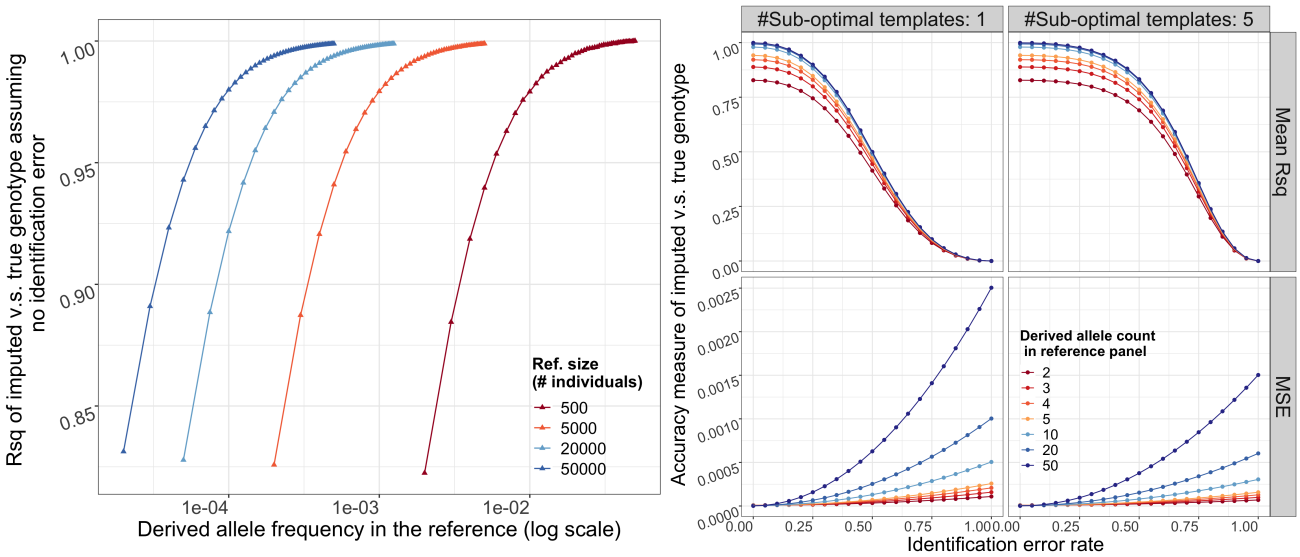

(a) Average theoretical r^2.

(b) r^2 and MSE changes with identification error.

Figure 3: a) The upper bound of squared correlation (r^2) (y-axis) between imputed and true genotype dosages, conditional on the derived allele frequency in the reference (x-axis). Color indicates the size of reference panel. b) The r^2 (top) and MSE (bottom) when a certain proportion of weight (x-axis) is attributed to sub-optimal templates. The impact depends on the absolute number of sub-optimal templates, we show examples of 1, 5 in the left and right columns. Here we fix the reference size to $20k$. Results are from $50k$ independent coalescence simulations, each data point is an average of over 10^7 loci.

Ref. Size (Individuals)	Derived allele count in the reference panel														
	2			3			5			10			20		
	Imputed dosage for the derived allele														
	> 0	> 0.5	$= 1$	> 0	> 0.5	$= 1$	> 0	> 0.5	$= 1$	> 0	> 0.5	$= 1$	> 0	> 0.5	$= 1$
500	2145	1122	848	1802	1006	653	1361	815	420	840	541	153	435	292	57
5000	214	109	80	179	97	60	136	78	41	84	52	23	49	32	13
20000	53	27	18	44	24	15	34	19	11	21	13	7	12	7	4
50000	21	10	7	17	9	6	13	8	4	8	5	3	5	3	2

Table 3: Consider imputing a sample dataset with one million individuals using a reference panel containing 500 to 50000 individuals from the same population as the sample, the expected number of individuals who are homozygous for the ancestral allele ($g = 0$) but have an imputed genotype dosage $\hat{g}$ as $\hat{g} > 0$, $\hat{g} > 0.5$ or $\hat{g} = 1$. Each combined column represents one derived allele count in the reference. Results are from $50k$ independent coalescence simulations, each data point is an average of over 10^7 loci.

To summarize the impact of this error on association tests, we calculated the squared correlation coefficient (r^2) between the imputed dosages and the true genotypes using simulations, both under the assumption that model misspecification is the only source of error and under the assumption that some reference haplotypes are falsely identified as being most closely related. r^2 is a commonly used measure for imputation quality, as it is directly related to statistical power in downstream association tests [5, 7, 22].

Still assuming that most closely related haplotypes are identified perfectly, we generated the distribution of expected r^2 for a range of minor allele counts and reference sizes using simulations

bioRxiv preprint doi: https://doi.org/10.1101/2020.08.10.245043; this version posted August 12, 2020. The copyright holder for this preprint (which was not certified by peer review) is the author/funder, who has granted bioRxiv a license to display the preprint in perpetuity. It is made available under aCC-BY-NC 4.0 International license.

(see the Method). The expected r^2 increases monotonically with derived allele frequency in the reference and reference size (Figure 3). If we consider the increase with DAF across reference sizes, we observe that the curves of expected r^2 values look very similar for each reference panel size, only shifted by a factor of 1/panel size. In other words, r^2 of variants with the same minor allele count remains almost the same across all considered reference sizes. For example, the average r^2 among doubletons is 0.822 in a reference size of 500 and 0.831 in a reference sample size of 50,000, where its frequency is only 1/100 of the former. For variants observed ten or more times in the reference, the expected r^2 is > 0.97 regardless of the size of the reference, as model misspecification do not play a mayor role for the imputation quality of these variants.

To include other sources of error in the imputation process, we model the false identification of reference haplotypes that are more distantly related to the target as templates. Those distantly related haplotypes are less likely to carry the same allele as the target haplotype and thus introduce an additional source of error. We parameterize this identification error as the sum of all probabilities assigned to falsely identified templates, denoted as q (see the Method). In practice, this imputation error depends on the choice of imputation algorithm, marker density, quality of genotyping and statistical phasing; detailed modeling of these factors is beyond the scope of this paper.

As expected, imputation error of the variant increases with increasing q shown as the mean squared error (MSE) of the imputed genotype (Figure 3b). As the imputed genotype for all individuals converges to the allele frequency f as q goes to 1, the MSE increases faster with higher f. Similarly, the r^2 between the true genotype and the imputed genotype decreases with increasing q. However, including some suboptimal haplotypes only has a small effect for rare variants. If we assume a single sub-optimal template, $q < 10\%$ only has marginal effect on r^2, when q increases beyond this threshold the decrease of r^2 becomes almost linear. This threshold depends on the number of sub-optimal templates: with a larger number of templates, the variance of the imputed genotype decreases and the effect of including suboptimal templates is more deterministic (see the Method). Accordingly, if the number of suboptimal templates is larger, the threshold where r^2 starts

bioRxiv preprint doi: https://doi.org/10.1101/2020.08.10.245043; this version posted August 12, 2020. The copyright holder for this preprint (which was not certified by peer review) is the author/funder, who has granted bioRxiv a license to display the preprint in perpetuity. It is made available under aCC-BY-NC 4.0 International license.

to decrease with q is larger while the MSE is lower (Figure 3b). For example, consider imputing a variant that is a doubleton in the reference with 20k haplotypes. Assuming no identification error, $r_0^2 = 0.83$. If we identify one sub-optimal templates with posterior probability 0.3 as well as all most closely related haplotypes, the expected r^2 is 0.70 and the MSE is 1.80×10^{-5}. If we instead identify 5 sub-optimal templates with total posterior probability 0.3 as well as all most closely related haplotypes, the expected r^2 increases to 0.80 while the MSE decreases to 1.44×10^{-5}.

For variants with derived allele count < 5 in the reference, the error caused by model misspecification dominates for a wide range of q; while for variants of derived allele count over 20 the error caused by model misspecification is negligible and the r_0^2 with perfectly identified optimal templates is above 0.99 regardless of the reference size (Table 4), thus the identification error dominates the empirical imputation error.

Ref. Size	Derived allele count in the reference					
(Individuals)	2	3	4	5	10	20
500	0.822(0.089)	0.885(0.067)	0.919(0.051)	0.940(0.041)	0.979(0.017)	0.995(0.0055)
2000	0.823(0.089)	0.886(0.066)	0.920(0.051)	0.940(0.040)	0.979(0.016)	0.994(0.0054)
5000	0.826(0.088)	0.887(0.065)	0.921(0.050)	0.941(0.040)	0.979(0.016)	0.994(0.0055)
20000	0.828(0.087)	0.889(0.065)	0.922(0.050)	0.942(0.040)	0.980(0.016)	0.994(0.0053)
50000	0.831(0.087)	0.891(0.065)	0.923(0.050)	0.943(0.039)	0.980(0.016)	0.994(0.0053)

Table 4: The maximal squared correlation can be achieved. Numbers in the parentheses are standard deviation summarized over 10^7 loci, representing the variation among variants in a population sample. Results are from $50k$ independent coalescence simulations.

3.3 Length between template switches

We now consider another potential source of error in current imputation model: the switch between templates. When we model the target haplotype as a mosaic of templates from the reference, switching between templates can be interpreted as a historical recombination event that breaks the genealogical bond between the target and its current template, i.e., the branches connecting the two leaves in a coalescent tree. The two haplotypes will become practically independent beyond the recombination break point.

Conditional on a known local genealogy, the length to the next recombination break point follows

bioRxiv preprint doi: https://doi.org/10.1101/2020.08.10.245043; this version posted August 12, 2020. The copyright holder for this preprint (which was not certified by peer review) is the author/funder, who has granted bioRxiv a license to display the preprint in perpetuity. It is made available under aCC-BY-NC 4.0 International license.

an exponential distribution, with the rate proportional to twice the time to the most recent common ancestor (TMRCA) between the target and the template. In practice, the genealogy is unknown, and the length to the next recombination break point is a combination of the distribution of the conditional length and the time to the TMRCA (detailed in Method). Here we compare this mixture distribution with the exponential distribution that is typically assumed in current imputation methods [11, 2].

Comparing the mixture distribution to an exponential distribution with the same mean shows that with genealogy and population history aware modeling, the distribution of length between switches is very similar for small reference samples ($n = 500$) (Figure 4). For larger reference samples ($n = 20,000$) the mixture distribution has larger variance, with higher density in both extremely short and long intervals but lower density for intermediate ones. If the excess of short no-recombination intervals is not well captured due to model misspecification, we expect to have more suboptimal templates thus higher imputation error rate. When the reference size increases, switches are less frequent as it is more likely to find a template sharing a very recent MRCA with the target.

bioRxiv preprint doi: https://doi.org/10.1101/2020.08.10.245043; this version posted August 12, 2020. The copyright holder for this preprint (which was not certified by peer review) is the author/funder, who has granted bioRxiv a license to display the preprint in perpetuity. It is made available under aCC-BY-NC 4.0 International license.

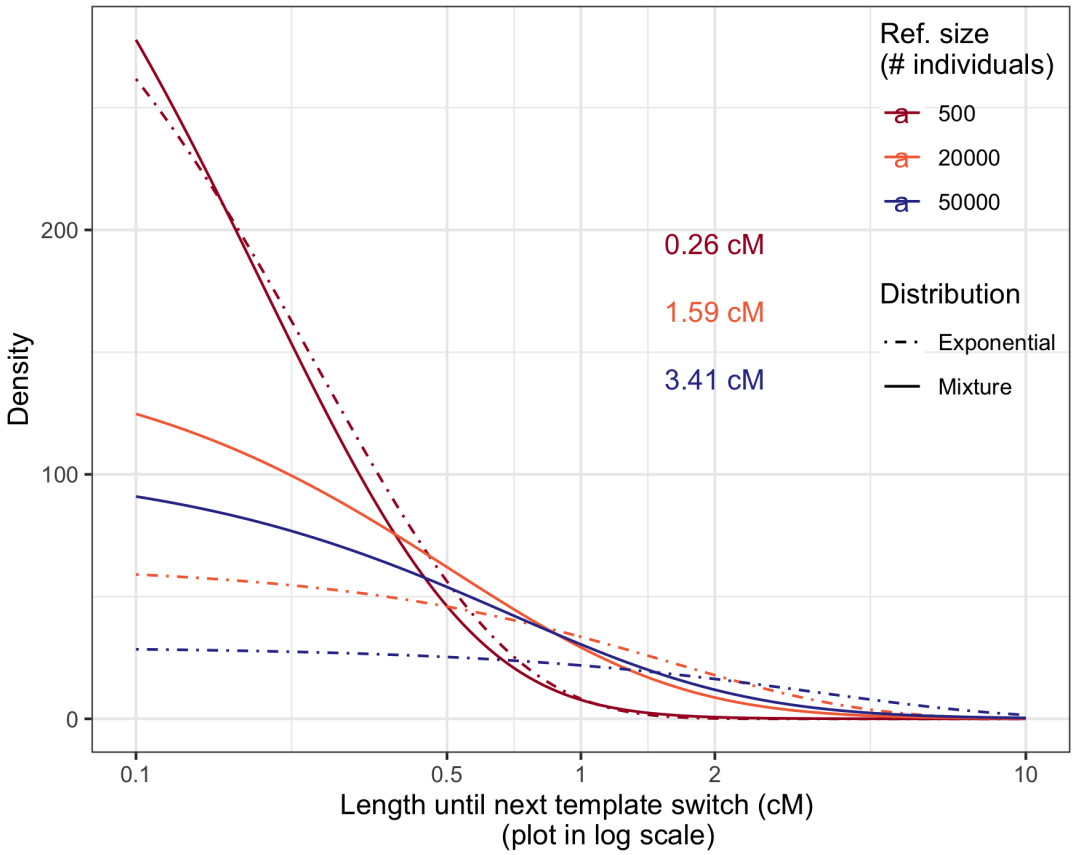

Figure 4: Distribution of the distance before the next recombination event breaking the relation between a pair of haplotypes. The x-axis shows the length in genetic distance (cM). Solid line is predicted by our coalescent model, the dashed line is an exponential distribution with the same mean as we predicted. Colors represent different reference sizes (n) in the number of individuals. The average lengths with reference being n=500, 20000, 50000 are 0.26, 1.59 and 3.41 cM respectively.

bioRxiv preprint doi: https://doi.org/10.1101/2020.08.10.245043; this version posted August 12, 2020. The copyright holder for this preprint (which was not certified by peer review) is the author/funder, who has granted bioRxiv a license to display the preprint in perpetuity. It is made available under aCC-BY-NC 4.0 International license.

4 Discussion

The empirical performance of imputation methods has been extensively studied [3, 23, 17, 4], while the theoretical behavior and limit of the underlying framework has not been well characterized, especially for rare variants. We formulate this problem of imputation accuracy into a coalescent model, considering imputing the missing genotypes on one target haplotype by copying from a set of reference haplotypes that share the most recent common ancestor (MRCA) with the target. Our approach identifies two model misspecifications in modern imputation algorithms and explores their impact on our ability to impute rare variants.

First, most imputation algorithms model a single best template as the hidden variable to infer. We show that, in 1/3 of the cases, multiple haplotypes are equally good templates for imputing one target in any given reference panel, independent of reference sample size or population history. The resulting model misspecification leads to imputation error when genetic variants are shared by some of the optimal templates but not with the target. We develop analytical expressions for the imputation error resulting from this model misspecification as a function of the derived allele frequency and reference size.

For this purpose, we assume that the imputation algorithm correctly identifies the most closely related haplotypes so that this model misspecification is the only source of error. In this idealized scenario, we observe that for variants observed five or less times in the reference panel, $> 8\%$ of variants with non-zero dosage are non-carriers; up to minor allele count 10, the mean r^2 between the imputed dosage and true genotypes < 0.98. Conditional on the derived allele count, this effect is broadly independent of reference panel size: although the probability of falsely imputing carriers of the rare allele decreases as the reference panel size becomes large, the number of true carriers also decreases and the proportion of false carriers over true carriers stays about the same. Including other sources of error that occur in practice further decreases imputation accuracy. Thus the expected r^2 we present here designate the upper bound of achievable mean imputation accuracy for rare variants in current imputation framework.

bioRxiv preprint doi: https://doi.org/10.1101/2020.08.10.245043; this version posted August 12, 2020. The copyright holder for this preprint (which was not certified by peer review) is the author/funder, who has granted bioRxiv a license to display the preprint in perpetuity. It is made available under aCC-BY-NC 4.0 International license.

Such imputation error substantially reduces the power for detecting novel risk variants in an association study based on imputed genotypes. Two scenarios can be considered here: First, single-marker tests of imputed rare variants can be powerful if the case-control data set is much larger than the imputation panel [23]. In this scenario, inaccurately inferred genotypes at a disease-related locus attenuate the allele frequency difference between cases and controls, and r^2 is directly related to this loss of information that compromises the statistical power in association tests. Imputation error rate of $2\% \sim 6\%$ leads to $10\% \sim 60\%$ increase in required sample size in a single marker test [7]. As a second scenario, imputed rare variants can be aggregated into a single test statistic [10]. In this study design, poorly imputed variants will have an attenuated signal, potentially diluting the signal from better imputed variants. This loss of power can be limited by focusing on imputed variants where misspecification will not impede imputation accuracy, e.g. variants that occur more than five times in the reference.

We consider a second model misspecification: the use of exponential distributions to model the length of contiguous haplotypes without template switches. The true distribution of this length is driven both by the recombination rate and the relationship between the template haplotype and the target haplotype. For small reference sample sizes such as 1000 genomes[1] this model misspecification has a negligible effect, but for reference samples of the scale of TopMed[23] or the Haplotye Reference Consortium[12], the length distribution of shared segments between the target and a single template has a much heavier tails than modelled. This misspecification penalizes both extremely short and extremely long switching intervals, decreasing the probability of finding the optimal templates. This in turn reduces imputation accuracy, especially for low frequency variants beyond the effect of the first model misspecification described above.

Results we present here are broadly robust to assumptions about population size history in a range reasonable for major human populations. We assume that the imputed region is evolutionary neutral; for loci under selection the impact of the described model misspecifications would likely depend both on the selection model and on the population history. Further, we assume that the

bioRxiv preprint doi: https://doi.org/10.1101/2020.08.10.245043; this version posted August 12, 2020. The copyright holder for this preprint (which was not certified by peer review) is the author/funder, who has granted bioRxiv a license to display the preprint in perpetuity. It is made available under aCC-BY-NC 4.0 International license.

reference is from the same homogeneous population as the target sample. If we instead modeled a diverse reference sample, results would depend on the frequency distribution of the imputed variant among the reference samples. For rare alleles, which are typically private to a single population, only members of that single population among the reference would affect imputation accuracy. Our results can be extended to including migration, admixture or selection, as the mathematical derivation and simulation scheme in this work are general for coalescence at a single locus.

Overall, we identify that the model misspecifications in imputation algorithms limit our ability for imputing rare variants, reducing the power of single marker tests in studies that impute rare variants into very large target datasets. Moreover, rare variant aggregation tests of imputed rare variants may lose power, especially if they focus on alleles that are observed only a few times in the reference panel. Beyond improving our understanding of the performance of imputation algorithms, these results should allow us to improve imputation algorithms and thus identify new risk variants. Our results suggest that potential improvement of the imputation framework may lie in more detailed modeling of the underlying genealogy, especially for extremely rare variants where only a small subset of the reference contribute information about the imputed genotype.

Software Availability

Codes used to perform analytical calculation and coalescent simulation are available from `https://github.com/Yichen-Si/ImputationBound`.

Acknowledgements

We thank Noah Rosenberg and Jonathan Terhorst for thoughtful comments. Funding for this research was provided by US National Institutes of Health (NIH) US National Institutes of Health grant R01 HG005855.

bioRxiv preprint doi: https://doi.org/10.1101/2020.08.10.245043; this version posted August 12, 2020. The copyright holder for this preprint (which was not certified by peer review) is the author/funder, who has granted bioRxiv a license to display the preprint in perpetuity. It is made available under aCC-BY-NC 4.0 International license.

A Probability distribution of fractional dosages

In the Method section, we derived the probability of having even the best possible evidence suggesting a wrong allele type. Here we will generalize it to the cases where the most closely related templates have different allele types, resulting in a fractional estimated dosage (figure 1b).

Let $P(\hat{g} = j/u, g = 0|j; n)$ be the probability of having u equally good optimal templates, j of which carrying the mutation, for a target actually carrying the ancestral allele; conditional on observing the derived allele count as j. Let (k', d') denote the numbers of ancestral lines within the size u subtree when the branch carrying the mutation starts and ends; (k'', d'') denote the numbers of lines in the whole tree at the corresponding time point.

We will outline the calculation of the joint probability (the numerator), while the denominator is the same unfolded frequency spectrum as before. We proceed by the following steps, each subsequent probability is conditional on the previous one, in parallel with that for the special case in the Method.

1) The target haplotype does not coalesce in the first $(n - d)$ events: $P_0(n + 1, d + 1)$.

2) A branch of size u arises in the reference at the $(n-k)$th event, then remains alone till the $(n-d)$th event to coalesce with that external branch: $P(u, k, d; n)P_0(k, d + 1)\frac{1}{\binom{d+1}{2}}$.

3) The subtree of size u contains a branch of size j: $P(j|u; n) = \sum_{(k',d')} P(j, k', d'|u; n)$. (This step only concerns the topology within the subtree)

4) The size-j branch encounters a mutation:$P(m \geq 1|j, k', d', u, k, n) = \sum_{(k'',d'')} P(m \geq 1|k'', d''; n + 1)P(k'', d''|k', d', u, k, n)$. (Here we need to put the subtree back to the whole size-$(n + 1)$ tree to get the branch length and introduce mutation)

Step 1-2) are similar to the three steps in the previous section except for not involving mutation events, we combine them to $P(ext, u, k, d; n)$: an external branch first coalesces at the $(n-d)$th event with an internal branch of size u which starts at the $(n - k)$th event. In step 3), $P(j, k', d'|u; n)$ is similar to $P(u, k, d; n)$ in step 2), as $P(j, k', d'|u; n) = P(j, k', d'; u)$: the probability for a branch of

bioRxiv preprint doi: https://doi.org/10.1101/2020.08.10.245043; this version posted August 12, 2020. The copyright holder for this preprint (which was not certified by peer review) is the author/funder, who has granted bioRxiv a license to display the preprint in perpetuity. It is made available under aCC-BY-NC 4.0 International license.

size j to start at the $(u-k')$th event and end at the $(u-d')$th event.

$$
\begin{aligned}
&P(\hat{g}=j/u,\ g=0,\ j;n)\\
&=\sum_{(k,d)} P(ext,u,k,d;n)P(m\geq 1,j|u,k,d;n)\\
&=\sum_{(k,d)} P(ext,u,k,d;n)\left\{\sum_{(k',d')}\left[P(j,k',d'|u,k;n)\sum_{(k'',d'')}P(m\geq 1|k'',d'';n+1)P(k'',d''|k',d',u,k,n)\right]\right\}\\
&(\sum_{(k,d)}=\sum_{k=2}^{n-u+1}\sum_{d=1}^{k};\quad \sum_{(k',d')}=\sum_{k'=2}^{u-j+1}\sum_{d'=1}^{k'-1};\quad \sum_{(k'',d'')}=\sum_{k''=k'+1}^{n-u+k'}\sum_{d''=d'+k-1}^{k''-1}.)
\end{aligned}
\tag{16}
$$

The only component left is $P(k'',d''|k',d',u,k,n)$, the link between the topology within the subtree and the branch lengths, which is relative to the whole sample and involves the population size history model. Since coalescent time intervals are measured for the whole tree, (k'',d'') tells us when the branch of size j starts and ends, which leads to the probability for a mutation to occur.

We divide the coalescent process among the whole reference from n lines to k lines into three parts: $n\to k''\to d''\to k$. There are $(n-k''-1)+(k''-d''-1)+(d''-k-1)$ unfixed events (since we are conditioning on the three time points, (k',k''), (d',d'') and (k)). Within each part, we consider the number of events that has to happen inside the subtree: $(u-k'-1),(k'-d'-1),(d'-1-1)$. With the number of lines fixed, $P(k'',d''|k',d',u,k,n)$ is calculated by considering the possible ways to arrange those events in the three time intervals.

$$
P(k'',d''|k',d',u,k,n)=\frac{\binom{n-k''-1}{u-k'-1}\binom{k''-d''-1}{k'-d'-1}\binom{d''-k-1}{d'-2}}{\binom{n-k-1}{u-2}}
\tag{17}
$$

The denominator in (10) comes from removing the constrains introduced by the mutation event. Conditional on (u,k), there are in total $(n-k-1)$ unfixed events in the whole tree, including $(u-2)$ in the subtree. Since (k'',d'') defines the coalescent time in the whole size-$(n+1)$ tree, we can calculate the length of the branch carrying mutation by (6): $P(m\geq 1|k'',d'';n+1)=\mu\sum_{i=d''+2}^{k''+1}E[T_i;n+1]$.

bioRxiv preprint doi: https://doi.org/10.1101/2020.08.10.245043; this version posted August 12, 2020. The copyright holder for this preprint (which was not certified by peer review) is the author/funder, who has granted bioRxiv a license to display the preprint in perpetuity. It is made available under aCC-BY-NC 4.0 International license.

B Population growth model does not make qualitative difference

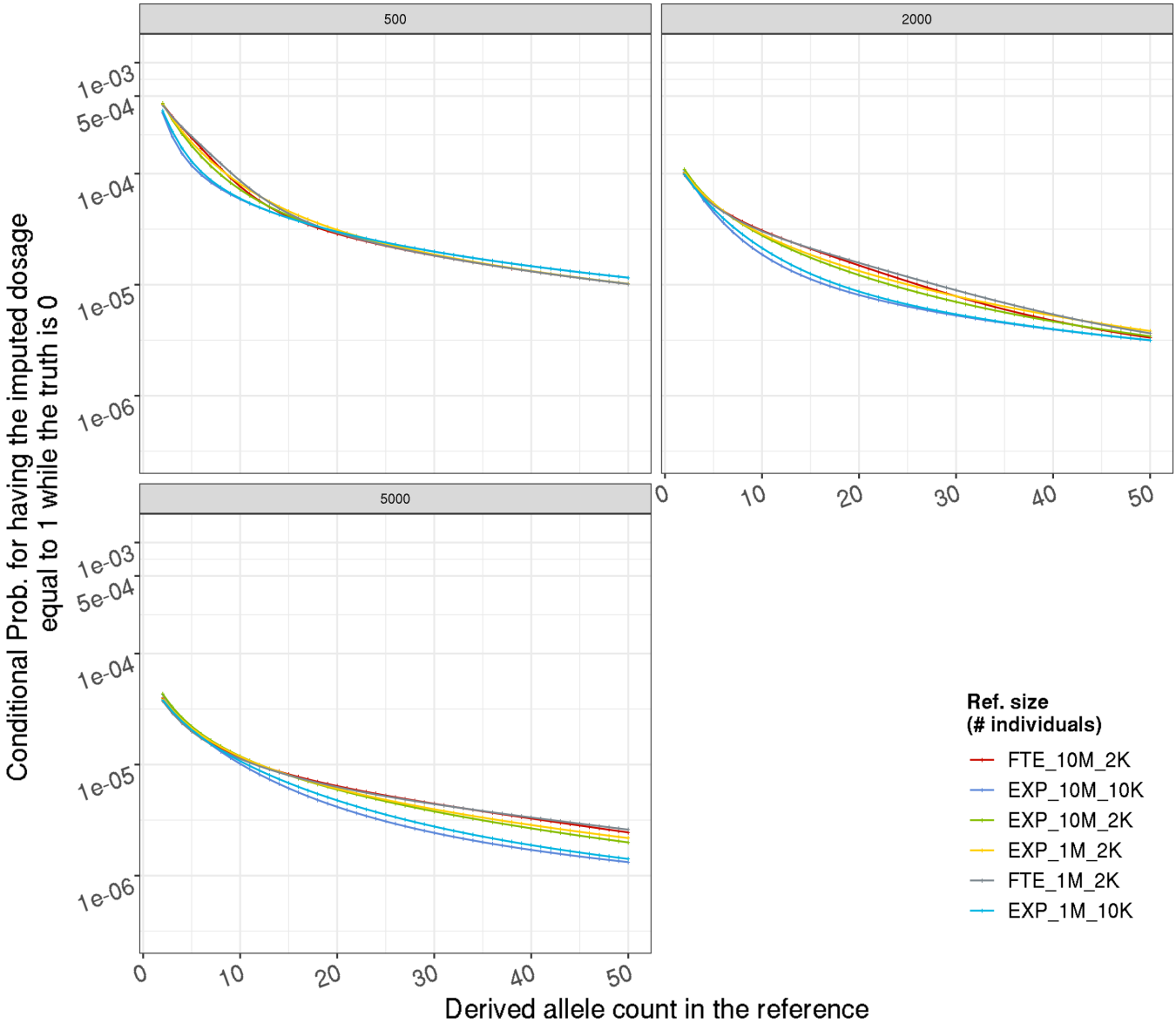

Figure 5: Effect of population growth model on false discovery rate among non-carriers, from analytical calculation. Given a target haplotype carrying the ancestral allele, the probability (y-axis, in log scale) of having all the most closely related reference haplotype in the reference panel carrying the derived allele thus an estimated dosage 1, on the derived allele frequency in the reference (x-axis). Each sub-figure represents one reference size (in individual); each color represents a population growth model. FTE(EXP)_10M_2K: faster-than-exponential (exponential) growth with current day effective population size 10 millions, and a bottleneck with effective population size 2 thousands.

bioRxiv preprint doi: https://doi.org/10.1101/2020.08.10.245043; this version posted August 12, 2020. The copyright holder for this preprint (which was not certified by peer review) is the author/funder, who has granted bioRxiv a license to display the preprint in perpetuity. It is made available under aCC-BY-NC 4.0 International license.

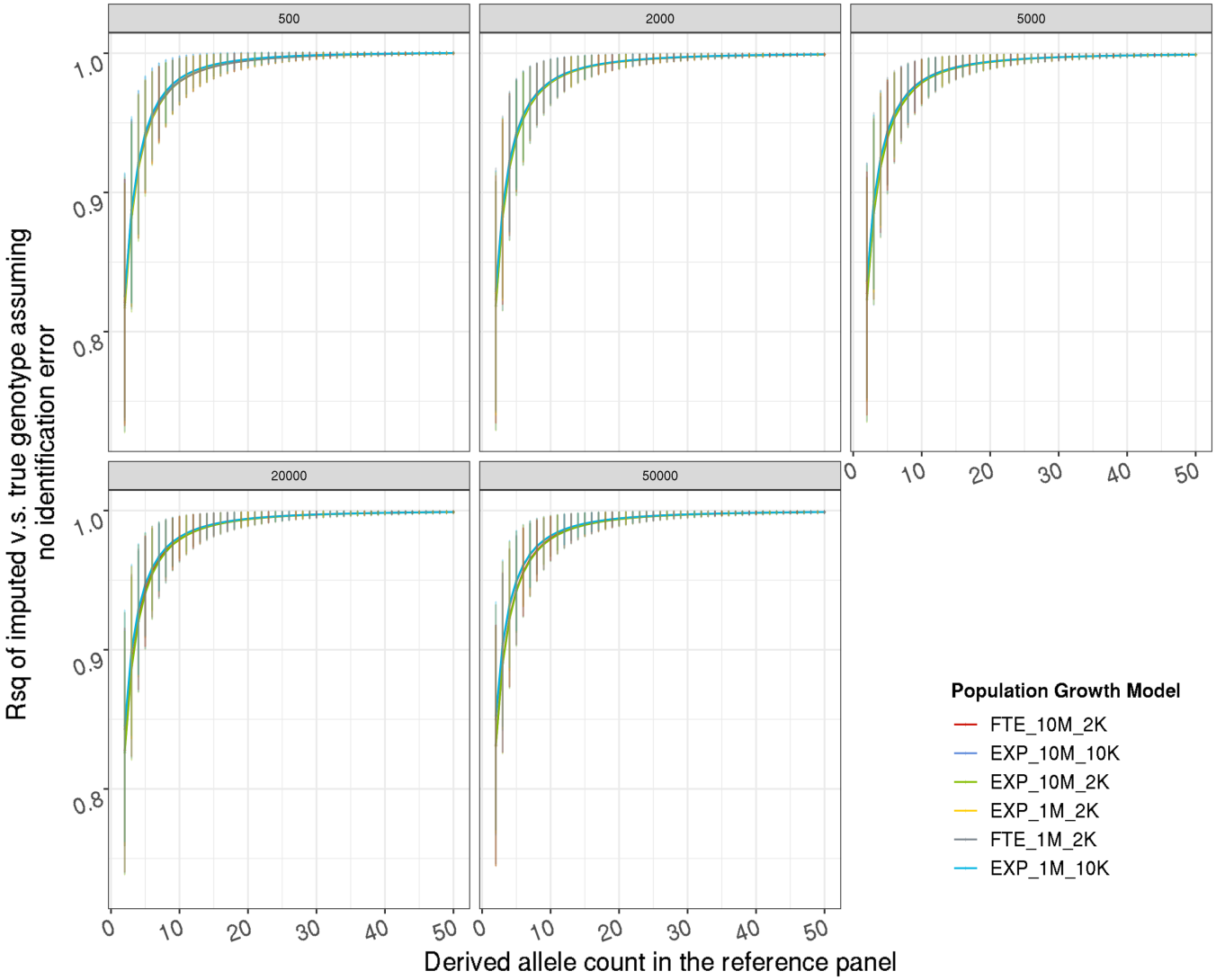

Figure 6: Effect of population growth model on imputation accuracy upper bound (r^2), from coalescent simulation. Y-axis is the average r^2 between imputed dosages and true genotypes without identification error; error bars represent one standard deviation. Each sub-figure represents one reference size (in individual); each color represents a population growth model. FTE(EXP)_10M_2K: faster-than-exponential (exponential) growth with current day effective population size 10 millions, and a bottleneck with effective population size 2 thousands.

bioRxiv preprint doi: https://doi.org/10.1101/2020.08.10.245043; this version posted August 12, 2020. The copyright holder for this preprint (which was not certified by peer review) is the author/funder, who has granted bioRxiv a license to display the preprint in perpetuity. It is made available under aCC-BY-NC 4.0 International license.

References

[1] David L. Altshuler et al. "A map of human genome variation from population-scale sequencing". In: *Nature* 467.7319 (2010), pp. 1061–1073. ISSN: 14764687. DOI: 10.1038/nature09534.

[2] Brian L. Browning, Ying Zhou, and Sharon R. Browning. "A One-Penny Imputed Genome from Next-Generation Reference Panels". In: *The American Journal of Human Genetics* 103.3 (2018), pp. 338–348. ISSN: 00029297. DOI: 10.1016/j.ajhg.2018.07.015. URL: https://linkinghub.elsevier.com/retrieve/pii/S0002929718302428.

[3] Ariel W. Chan, Martha T. Hamblin, and Jean-Luc Jannink. "Evaluating Imputation Algorithms for Low-Depth Genotyping-By-Sequencing (GBS) Data". In: *PLOS ONE* 11.8 (Aug. 2016). Ed. by Frank Alexander Feltus, e0160733. ISSN: 1932-6203. DOI: 10.1371/journal.pone.0160733. URL: http://dx.plos.org/10.1371/journal.pone.0160733.

[4] Sayantan Das et al. "Next-generation genotype imputation service and methods". In: *Nature Genetics* 48.10 (2016), pp. 1284–1287. ISSN: 15461718. DOI: 10.1038/ng.3656. arXiv: 15334406.

[5] Yongtao Guan and Matthew Stephens. "Practical Issues in Imputation-Based Association Mapping". In: *PLoS Genetics* 4.12 (2008). DOI: 10.1371/journal.pgen.1000279.

[6] Lucy Huang, Erkan O. Buzbas, and Noah A. Rosenberg. "Genotype imputation in a coalescent model with infinitely-many-sites mutation". In: *Theoretical Population Biology* 87.1 (2013), pp. 62–74. ISSN: 00405809. DOI: 10.1016/j.tpb.2012.09.006. URL: http://dx.doi.org/10.1016/j.tpb.2012.09.006.

[7] Lucy Huang, Chaolong Wang, and Noah A Rosenberg. "The Relationship between Imputation Error and Statistical Power in Genetic Association Studies in Diverse Populations". In: *The American Journal of Human Genetics* 85.5 (2009), pp. 692–698. ISSN: 0002-9297. DOI: 10.1016/j.ajhg.2009.09.017. URL: http://dx.doi.org/10.1016/j.ajhg.2009.09.017.

bioRxiv preprint doi: https://doi.org/10.1101/2020.08.10.245043; this version posted August 12, 2020. The copyright holder for this preprint (which was not certified by peer review) is the author/funder, who has granted bioRxiv a license to display the preprint in perpetuity. It is made available under aCC-BY-NC 4.0 International license.

[8] Ethan M. Jewett et al. "A coalescent model for genotype imputation". In: *Genetics* 191.4 (2012), pp. 1239–1255. ISSN: 00166731. DOI: 10.1534/genetics.111.137984.

[9] J. F. C. Kingman. "On the Genealogy of Large Populations". In: *Journal of Applied Probability* 19.A (1982), pp. 27–43. DOI: doi:10.2307/3213548. URL: www.jstor.org/stable/3213548.

[10] Seunggeung Lee et al. "Rare-variant association analysis: Study designs and statistical tests". In: *American Journal of Human Genetics* 95.1 (2014), pp. 5–23. ISSN: 15376605. DOI: 10.1016/j.ajhg.2014.06.009.

[11] Na Li and Matthew Stephens. "Modeling Linkage Disequilibrium and Identifying Recombination Hotspots Using Single-Nucleotide Polymorphism Data". In: *Genetics* 165.4 (2003), pp. 2213–2233.

[12] Shane McCarthy et al. "A reference panel of 64,976 haplotypes for genotype imputation". In: *Nature Genetics* 48.10 (2016), pp. 1279–1283. ISSN: 15461718. DOI: 10.1038/ng.3643.

[13] Joshua S Paul, Matthias Steinrucken, and Yun S. Song. "An Accurate Sequentially Markov Conditional Sampling Distribution for the Coalescent With Recombination". In: *Genetics* (2011). DOI: 10.1534/genetics.110.125534.

[14] Andrzej Polanski et al. "Coalescence computations for large samples drawn from populations of time-varying sizes". In: *PLoS ONE* 12.2 (2017), pp. 1–22. ISSN: 19326203. DOI: 10.1371/journal.pone.0170701.

[15] Mark Reppell, Michael Boehnke, and Sebastian Zollner. "The Impact of Accelerating Faster than Exponential Population Growth on Genetic Variation". In: *Genetics* 196.March (2014), pp. 819–828. DOI: 10.1534/genetics.113.158675.

[16] Bertrand Servin and Matthew Stephens. "Imputation-based analysis of association studies: Candidate regions and quantitative traits". In: *PLoS Genetics* 3.7 (2007), pp. 1296–1308. ISSN: 15537390. DOI: 10.1371/journal.pgen.0030114.

bioRxiv preprint doi: https://doi.org/10.1101/2020.08.10.245043; this version posted August 12, 2020. The copyright holder for this preprint (which was not certified by peer review) is the author/funder, who has granted bioRxiv a license to display the preprint in perpetuity. It is made available under aCC-BY-NC 4.0 International license.

[17] Shuo Shi et al. "Comprehensive Assessment of Genotype Imputation Performance". In: *Human Heredity* 83.3 (2018), pp. 107–116. ISSN: 0001-5652. DOI: 10.1159/000489758. URL: https://www.karger.com/Article/FullText/489758.

[18] Leo Speidel et al. "A method for genome-wide genealogy estimation for thousands of samples". In: *Nature Genetics* 51.September (2019). ISSN: 1546-1718. DOI: 10.1038/s41588-019-0484-x.

[19] Jonathan Terhorst, John A. Kamm, and Yun S. Song. "Robust and scalable inference of population history from hundreds of unphased whole genomes". In: *Nature Genetics* 49.2 (2017), pp. 303–309. ISSN: 15461718. DOI: 10.1038/ng.3748. URL: http://dx.doi.org/10.1038/ng.3748.

[20] Nicholas J. Timpson et al. "Genetic architecture: The shape of the genetic contribution to human traits and disease". In: *Nature Reviews Genetics* 19.2 (2018), pp. 110–124. ISSN: 14710064. DOI: 10.1038/nrg.2017.101. URL: http://dx.doi.org/10.1038/nrg.2017.101.

[21] Carsten Wiuf and Peter Donnelly. "Conditional Genealogies and the Age of a Neutral Mutant". In: *Theoretical Population Biology* 56.2 (1999), pp. 183–201. DOI: doi:10.1006/tpbi.1998.1411.

[22] Genevieve L Wojcik et al. "Imputation-Aware Tag SNP Selection To Improve Power for Large-Scale, Multi-ethnic Association Studies." In: *G3: Genes—Genomes—Genetics* (2018). ISSN: 2160-1836. DOI: 10.1534/g3.118.200502.

[23] A Zachary et al. "Sequencing of 53,831 diverse genomes from the NHLBI TOPMed Program". In: (2019). DOI: https://doi.org/10.1101/563866.